Author(s): Hossain, Md. Kamal; Plutenko, Maxym O.; Schachner, Jörg A.; Haukka, Matti; Mösch-Zanetti, Nadia C.; Fritsky, Igor O.; Nordlander, Ebbe

Title: Dioxomolybdenum(VI) complexes of hydrazone phenolate ligands -syntheses and activities in catalytic oxidation reactions

Year: 2021

Version: Published version

Journal of the Indian Chemical Society 98 (2021) 100006

Contents lists available at ScienceDirect

Journal of the Indian Chemical Society

journal homepage: www.editorialmanager.com/JINCS/default.aspx

Dioxomolybdenum(VI) complexes of hydrazone phenolate ligands - syntheses and activities in catalytic oxidation reactions

Md Kamal Hossain [a,b], Maxym O. Plutenko [c], Jörg A. Schachner [d], Matti Haukka [e], Nadia C. Mösch-Zanetti [d], Igor O. Fritsky [c], Ebbe Nordlander [a,*]

[a] *Chemical Physics, Department of Chemistry, Lund University, P.O. Box 124, SE-22100, Lund, Sweden*
[b] *Department of Chemistry, Jahangirnagar University, Savar, Dhaka, 1342, Bangladesh*
[c] *Department of Chemistry, National Taras Shevchenko University, Volodymyrska Street 64, 01601, Kyiv, Ukraine*
[d] *Institute of Chemistry, University of Graz, Schubertstraße 1, 8010, Graz, Austria*
[e] *Department of Chemistry, P.O. Box 35, University of Jyväskylä, FI-40014, Jyväskylä, Finland*

A R T I C L E I N F O

Keywords:
Dioxomolybdenum(VI) complexes
Hydrazone
Schiff base
Oxidation
Epoxidation
Sulfoxidation

A B S T R A C T

The new *cis*-dioxomolybdenum (VI) complexes $[MoO_2(L^2)(H_2O)]$ (**2**) and $[MoO_2(L^3)(H_2O)]$ (**3**) containing the tridentate hydrazone-based ligands (H_2L^2 = *N*'-(3,5-di-*tert*-butyl-2-hydroxybenzylidene)-4-methylbenzohydrazide and H_2L^3 = *N*'-(2-hydroxybenzylidene)-2-(hydroxyimino)propanehydrazide) have been synthesized and characterized via IR, ^{1}H and ^{13}C NMR spectroscopy, mass spectrometry, and single crystal X-ray diffraction analysis. The catalytic activities of complexes **2** and **3**, and the analogous known complex $[MoO_2(L^1)(H_2O)]$ (**1**) (H_2L^1 = *N*'-(2-hydroxybenzylidene)-4-methylbenzohydrazide) have been evaluated for various oxidation reactions, *viz*. oxygen atom transfer from dimethyl sulfoxide to triphenylphosphine, sulfoxidation of methyl-*p*-tolylsulfide or epoxidation of different alkenes using *tert*-butyl hydroperoxide as terminal oxidant. The catalytic activities were found to be comparable for all three complexes, but complexes **1** and **3** showed better catalytic performances than complex **2**, which contains a more sterically demanding ligand than the other two complexes.

1. Introduction

Oxygen atom transfer (OAT) processes attract considerable interest because of their importance in nature and their potential applications in industrial oxidation reactions, e.g. sulfoxidation processes [1–3]. In biological systems a large number of such reactions are catalysed by molybdopterin-dependent enzymes with active sites containing a molybdenum cofactor (Moco) [4–7]. In order to emulate and understand such biological reactions, a plethora of molybdenum (VI) and molybdenum (IV) complexes have been developed as structural and functional model complexes for molybdenum-containing cofactors [8–11]. Most such modelling studies involve the use of sulfur-containing ligands, as the various mononuclear molybdenum cofactors always contain the ligand molybdopterin, where a dithiolene unit of the pterin ligand chelates the molybdenum ion [12–15].

A number of molybdenum complexes that are based on sulfur-free ligands and reveal OAT/oxidation activities have been investigated [16–21]. Such ligands include, for example, tris(pyrazol)borates [16,17], β-ketiminates [18,19] and the salan-type ligands [20,21]. The latter class of ligands consists of tri- and tetradentate phenol-containing N,O-donor ligands. Several molybdenum (VI) dioxo complexes with tridentate Schiff base ligands, including salan ligands, catalyse oxo transfer between DMSO and different phosphines as well as the oxidation of benzoin to benzil [21–24].

Hydrazone-based ligands have attracted attention because of their versatile coordination properties and abilities to coordinate in both deprotonated and non-deprotonated forms [25,26] and their potential biological activities [27,28]. The results obtained with phenol-containing thiosemicarbazone ligands are particularly relevant [29]. A number of hydrazone complexes containing the *cis*-$Mo(VI)O_2$ entity have been prepared, and in some cases they have been investigated as catalysts for oxygen atom transfer processes [30–32].

Here we describe the synthesis and characterization of octahedral *cis*-$Mo(VI)O_2$ complexes based on three tridentate phenol-containing hydrazone ligands: *N*'-(2-hydroxybenzylidene)-4-methylbenzohydrazide (H_2L^1), *N*'-(3,5-di-*tert*-butyl-2-hydroxybenzylidene)-4-methylbenzohydrazide (H_2L^2) and *N*'-(2-hydroxybenzylidene)-2-(hydroxyimino)propanehydrazide (H_2L^3) (Fig. 1 and Scheme 1). The three ligands include a

* Corresponding author.
E-mail address: Ebbe.Nordlander@chemphys.lu.se (E. Nordlander).

https://doi.org/10.1016/j.jics.2021.100006
Received 27 November 2020; Accepted 8 January 2021

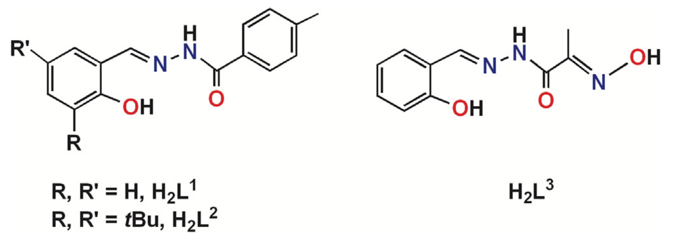

Fig. 1. Hydrazone ligands employed in this study.

potential O,N,O′-donor set formed by the amide and phenol oxygens, and the azomethine nitrogen atoms. The ligand H_2L^2 contains sterically bulky *tert*-butyl substituents in the aromatic ring (Fig. 1), while the ligand H_2L^3 is electron-depleted in comparison with H_2L^1 and H_2L^2 because of the presence of the oxime electron acceptor group. The potential of the molybdenum (VI) oxo complexes to effect catalytic oxygen atom transfer from dimethyl sulfoxide (DMSO) to a phosphine, sulfoxidation of methyl-*p*-tolylsulfide, and olefin epoxidation reactions are reported. The Mo(VI)O_2 complex of H_2L^1 has been previously reported by Lei et al. [25] but its catalytic activities have not been studied.

2. Results and discussion

All three complexes were synthesized following the procedure published by Lei et al. for the synthesis of $[MoO_2(L^1)(MeOH)]$ (**1**) [33]. The reaction of equimolar amounts of $[MoO_2(acac)_2]$ with H_2L^2 or H_2L^3 in (wet) methanol or methanol-water solutions afforded $[MoO_2(L^2)(H_2O)]$ (**2**) and $[MoO_2(L^3)(H_2O)]$ (**3**) (Scheme 1). Crystallization from the reaction mixtures at room temperature by slow evaporation of the solvent led to the formation of orange crystals in 69–85% yields. In these compounds, methanol (**1**) or water (**2**, **3**) is coordinated in the vacant coordination site. It should be noted that the methanol solvate analogue of **2**, $[MoO_2(L^2)(MeOH)]$, has been published recently [34].

The complexes were characterized by IR, ^{1}H and ^{13}C{^{1}H} NMR spectroscopy, ESI mass spectrometry and single crystal X-ray diffraction analysis of **2** and **3**. The complexes are stable at room temperature; they are well soluble in DMSO and DMF, and moderately soluble in methanol, chloroform and acetonitrile. The discussion below is restricted to the data for complexes **2** and **3**, as all relevant characterization data for **1** - including its crystal structure - have been published previously [33].

The hydrazone ligands are coordinated in their doubly deprotonated form to the metal center, *i.e.* via their phenolate substituent and the oxygen of the deprotonated amide group so that they become tridentate O,N,O′-donors. This is confirmed by the ^{1}H NMR and ^{13}C NMR spectra of the free ligands and their corresponding complexes. In the ^{1}H NMR spectrum of H_2L^3, the signals at δ 11.39 and 11.62 are attributed to the amide (RCONH) and aromatic OH groups, respectively. The disappearance of both peaks in the ^{1}H NMR spectrum of **3** indicates that both groups are deprotonated and coordinated to the molybdenum ion while the oxime NOH proton resonance is retained in the complex and is shifted to 12 ppm, which suggests that the oxime group remains protonated in the complex. In the ^{13}C NMR spectra of both **2** and **3**, the chemical shifts of the carbonyl, phenolate and methine carbon atoms are shifted to lower field in agreement with coordination of the ligands in the described manner.

The infrared spectra of complexes **2** and **3** showed shifts to lower wave numbers for the $\nu_{(C=O)}$ stretch of the amide group (1613 and 1604 cm^{-1} for **2** and **3**, respectively) in relation to the spectra of the corresponding free ligands, in agreement with coordination of the amide oxygen to the metal ion. The IR spectra also showed two strong bands around 916–920 and 944-954 cm^{-1} that are assigned as asymmetric and symmetric M = O stretches, respectively.

Solutions of complexes **2** in acetonitrile and **3** in methanol were studied by ESI mass spectrometry. The mass spectrum of **2** exhibits a molecular ion $[MoO_2(L^2)(H_2O)+MeCN]^+$ peak at $m/z = 551$ and a ligand molecular ion $[H_2L^2+Na]^+$ at $m/z = 389$. For complex **3**, a pattern corresponding to mononuclear $[MoO_2(L^3)]+H]^+$ ($m/z = 349.97$) was found. Furthermore, the formation of the associates of the mononuclear species with alkaline metal ions $\{[MoO_2(L^3)]+Na^+\}^+$ ($m/z = 371.95$) and $\{[MoO_2(L^3)]+K^+\}^+$ ($m/z = 387.93$) were also detected as predominant species. In addition, the ESI-MS spectrum of **3** revealed the presence of a pattern corresponding to the dinuclear species $[2\{MoO_2(L^3)\}+Na]^+$ ($m/z = 716$; Fig. S1, Supplementary Material).

3. Crystal and molecular structures of 2 and 3

The solid-state structures of $[MoO_2(L^2)(H_2O)]$ (**2**) and $[MoO_2(L^3)(H_2O)]\cdot 2H_2O$ (**3**·$2H_2O$) were determined by single crystal X-ray diffraction. Relevant crystallographic data for **2** and **3** are summarized in Table 1 and selected bond lengths and angles are given in Table 2. The molecular structures of **2** and **3** are shown in Fig. 2. The complexes are chiral with stereogenic centers at the molybdenum ions, but both enantiomers are present in the centrosymmetric monoclinic and triclinic structures.

The solid state structures confirm that the fully deprotonated hydrazone ligands coordinate by their phenolate O, azomethine N and enolic O atoms (O(1), N(2), O(2)) in a planar tridentate O,N,O′ fashion, imposing what is effectively a *mer* coordination geometry with the remaining three positions of the distorted octahedron occupied by the two oxido ligands and a coordinated water molecule. The Mo–O bond lengths fall in the range 1.6972(8)-1.7189(15) Å, which are typical for Mo(VI)=O double bonds, and the O(3)-Mo(1)-O(4) angles are also typical for *cis*-Mo(VI)O_2 entities (105.71 (7)° and 105.42 (4)° for **2** and **3**, respectively). The O(3) oxido ligand is located *trans* to the azomethine nitrogen, N(2), with

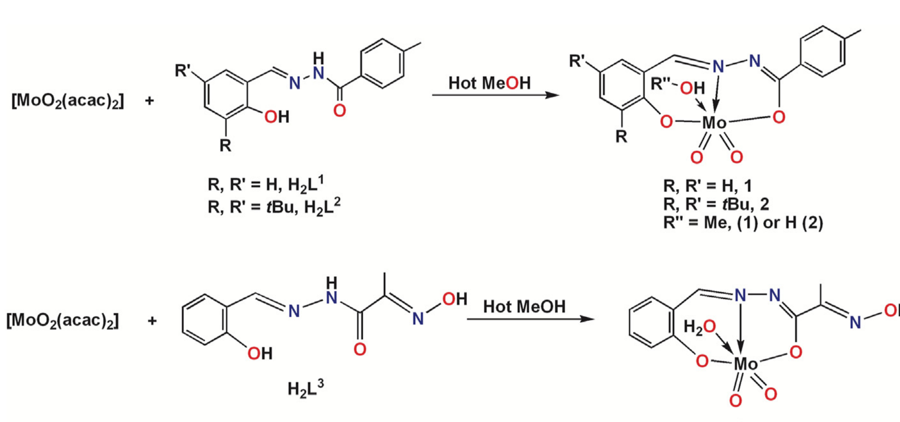

Scheme 1. Syntheses of complexes **1**–**3**.

Table 1
Summary of crystallographic data for $[MoO_2(L^2)(H_2O)]$ (**2**) and $[MoO_2(L^3)(H_2O)]\cdot 2H_2O$ (**3**·$2H_2O$).

	2	**3**·$2H_2O$
Empirical formula	$C_{23}H_{30}MoN_2O_5$	$C_{10}H_{15}MoN_3O_8$
Formula weight	510.43	401.19
Temperature (K)	123 (2)	170 (2)
Wavelength (Å)	1.54184	0.71073
Crystal system	Monoclinic	Triclinic
Space group	$P2_1/n$	P-1
a (Å)	9.44913 (13)	7.24920 (15)
b (Å)	21.6798 (3)	9.55895 (17)
c (Å)	11.33150 (16)	10.9038 (2)
α (°)	90	94.2393 (16)
β (°)	100.6173 (14)	108.402 (2)
γ (°)	90	90.9357 (16)
Volume ($Å^3$)	2281.57 (5)	714.35 (3)
Z	4	2
Density (calculated) ($Mg\ m^{-3}$)	1.486	1.865
μ (Mo K*α*) (mm^{-1})	5.006	0.964
F (000)	1056	404
Crystal size (mm)	0.20 × 0.03 x 0.03	0.38 × 0.23 x 0.05
θ range (°)	4.08 to 77.00	3.03 to 38.48
Limiting indices	$-9 \le h \ge 11$ $-27 \le k \ge 27$ $-13 \le l \ge 14$	$-12 \le h \ge 12$ $-16 \le k \ge 16$ $-19 \le l \ge 19$
Reflections collected	19797	28688
Independent reflections (R_{int})	4777 (0.0315)	7939 (0.0194)
Completeness to theta = 26.000°	99.1%	98.6%
Absorption correction	Semi-empirical from equivalents	Analytical
Max. and min. transmission	0.8701 and 0.4305	0.9500 and 0.7125
Refinement method	Full-matrix least-squares on F^2	Full-matrix least-squares on F^2
Data/restraints/parameters	4777/0/288	7939/0/208
Goodness of fit on F^2	1.039	1.140
Final *R* indices [$I > 2\sigma(I)$]	$R_1 = 0.0263$, $wR_2 = 0.0697$	$R_1 = 0.0191$, $wR_2 = 0.0544$
R indices (all data)	$R_1 = 0.0298$, $wR_2 = 0.0719$	$R_1 = 0.0210$, $wR_2 = 0.0558$
Largest difference in peak and hole (e $Å^{-3}$)	0.401 and −0.786	0.625 and −0.607

Table 2
Selected bond lengths (Å) and bond angles (°) for $[MoO_2(L^2)(H_2O)]$ (**2**) and $[MoO_2(L^3)(H_2O)]$ (**3**).

	2	**3**
Mo (1)–O (1)	2.0184 (14)	2.0397 (7) (Mo (1)–O (2))
Mo (1)–O (2)	1.9212 (14)	1.9164 (7) (Mo (1)–O (1))
Mo (1)–O (3)	1.7189 (15)	1.7156 (7)
Mo (1)–O (4)	1.6920 (15)	1.6972 (8)
Mo (1)–O (5)	2.3257 (14)	2.2685 (7)
Mo (1)–N (2)	2.2442 (16)	2.2419 (7)
O (1)-Mo (1)-O (2)	148.32 (6)	150.33 (3)
O (3)- Mo (1)–O (4)	105.71 (7)	105.42 (4)
O (4)- Mo (1)–O (2)	99.14 (7)	98.89 (4)
O (3)- Mo (1)–O (2)	101.66 (7)	106.55 (3)
O (4)- Mo (1)–O (1)	96.41 (7)	94.69 (4)
O (3)- Mo (1)–O (1)	100.41 (6)	94.93 (3)
O (4)- Mo (1)–O (5)	169.67 (6)	169.33 (3)
O (3)- Mo (1)–O (5)	83.61 (6)	84.88 (3)
O (4)- Mo (1)–N (2)	92.49 (7)	90.43 (3)
O (3)- Mo (1)–N (2)	161.01 (6)	159.99 (3)
O (2)- Mo (1)–N (2)	80.25 (6)	82.37 (3)
O (1)- Mo (1)–N (2)	71.63 (6)	71.23 (3)

similar O(3)-Mo(1)-N(2) angles of 161.01 (6)° for **2** and 159.99 (3)° for **3**. The other oxido group, O (4), sits *trans* to the coordinated water solvent molecule with O(4)-Mo(1)-O(5) angles of 169.67 (6)° for **2** and 169.33 (3)° for **3**, with the *cis* O(4)-Mo(1)-N(2) angles to the azomethine

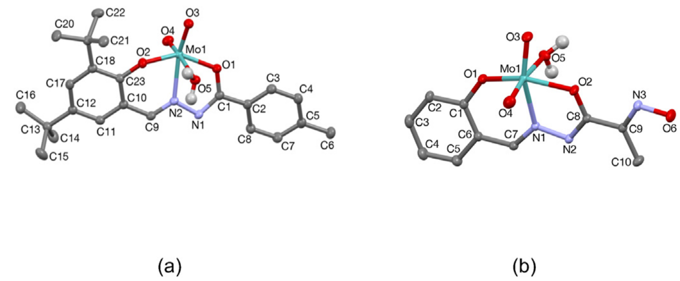

Fig. 2. Mercury plots of the molecular structures of (a) $[MoO_2(L^2)(H_2O)]$ (**2**) and (b) $[MoO_2(L^3)(H_2O)]$ (**3**) showing the atom numbering scheme. Hydrogen atoms (except for the aqua ligands) and solvent molecules have been omitted for the sake of clarity. Thermal ellipsoids are drawn at the 50% probability level.

nitrogen being close to those expected for an octahedron - 92.49 (7)° and 90.43 (3)° for **2** and **3**, respectively. The Mo-O_{water} and Mo–N distances Mo(1)–O(5) (2.3257 (14) Å for **2** and 2.2685 (7) Å for **3**) and Mo(1)–N(2) (2.2442 (16) Å for **2** and 2.2419 (7) Å for **3**) are elongated due the *trans* influence of the oxido ligands. The five-membered chelate rings Mo(1)-O(1)-C(1)-N(1)-N(2) are almost planar with N–N, N–C and C–O bond lengths that are typical for corresponding rings in other structurally characterized Mo(VI)O_2 hydrazone complexes [29,33,35–37].

Intermolecular hydrogen bond interactions are found in both crystal structures. The hydrogen bonding parameters for **2** and **3** are collected in Table 3. In the crystal structure of **2**, there is a strong intermolecular hydrogen bonding interaction between the coordinated water molecule and the oxido ligand O(3) with the O(5)-H(5B)···O $(3)^i$ (i = -x+1,-y+1,-z+1) distance being 2.765 (2) Å, and between the water molecule and the nitrogen of the azomethine-hydrazone fragment - O(5)-H(5A)···$N(1)^{ii}$ (ii = -x+2,-y+1,-z+1) = 2.825 (2) Å (Fig. 3).

In the crystal packing arrangement of **3**, the $[MoO_2(L^3)(H_2O)]$ molecule is connected with the neighboring identical molecule through two O(6)–H(6)···O(3) hydrogen bonds. In addition, these two molecules are connected through two co-crystallized water molecules with O(7)-H(7B)···O(2) and O(7)-H(7A)···N(3) intermolecular hydrogen bonds. These pairs are also connected through O(5)-H(5A)···N(2) hydrogen bonds forming a supramolecular 3-dimensional network along the *c* axis. The other hydrogen bonds, O(5)-H(5B)···O(8) and O(8)–H(8)···O(7) of the coordinated water, connect these chains, as well (Fig. 4).

4. Catalysis studies

4.1. Catalytic oxygen atom transfer

The reactivities of complexes **1**–**3** in catalytic oxygen atom transfer reactions were studied by using triphenylphosphine as an oxygen acceptor substrate. The reactions were performed in deuterated dimethyl sulfoxide (DMSO-d_6) that functioned as the ultimate oxygen donor (Scheme 2) and were monitored by ^{31}P NMR spectroscopy.

The studies on complexes **1**–**3** were carried out with low catalyst loadings (1 mol %) at 65 °C but the conversions were found to be very low for all catalysts after 24 h as well as after 48 h. After increasing the catalyst loadings to 5 mol%, complexes **1**–**3** gave conversions of approx. 65%, 20% and 85% after 20 h, and 90%, 40% and >99% after 40 h, respectively. The results are summarized in Table 4.

The catalytic activities for phosphine oxidation are thus clearly **3** > **1**>**2**, with **3** showing good activity and **1** acceptable activity. However, complex **2** showed poor activity. We attribute the poor catalytic efficiency of that complex to the steric hindrance of the *tert*-butyl substituents of the ligand, in particular the *tert*-butyl substituent in 6-position on the salicylaldimine ring.

Table 3
Hydrogen-bond parameters (Å,°) for the crystal structures of $[MoO_2(L^2)(H_2O)]$ (**2**) and $[MoO_2(L^3)(H_2O)]\cdot 2H_2O$ (**3**·$2H_2O$).

D-H···A	D-H (Å)	H···A (Å)	D···A (Å)	D-H···A (°)
2				
O(5)-H(5B)...O(3)^{i}	0.88	1.90	2.765 (2)	165.4
O(5)-H(5A) … N(1)^{ii}	0.88	1.99	2.825 (2)	157.2
3·$2H_2O$				
O(6)–H(6) … O(3)#1^{iii}	0.84	2.00	2.8126 (10)	161.9
O(5)-H(5A) … N(2)^{iv}	0.87	2.05	2.8825 (10)	159.8
O(7)-H(7A) … N(3)^{iii}	0.85	2.03	2.8675 (11)	170.4

Symmetry codes: (i) -x+1, -y+1, -z+1; (ii) -x+2, -y+1, -z+1; (iii) -x+1, -y+1, -z; (iv) -x+1, -y+1, -z+1.

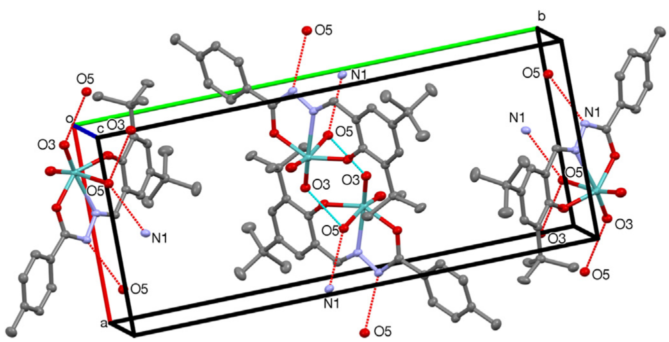

Fig. 3. A Mercury plot of the molecular packing of **2** viewed along the *c*-axis. Hydrogen bonds are shown as dashed lines.

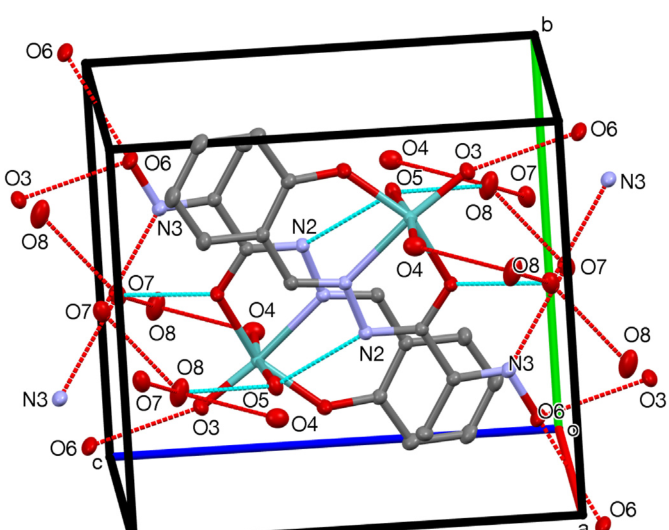

Fig. 4. A Mercury plot of the molecular packing of **3** viewed along the *a*-axis. Hydrogen bonds are shown as dashed lines.

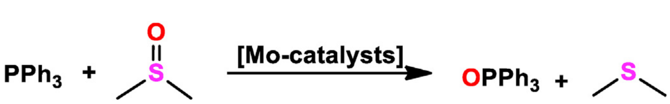

Scheme 2. Dioxidomolybdenum (VI) catalysed OAT reaction from DMSO to PPh_3.

4.2. Catalytic sulfoxidation

The oxidation of methyl-*p*-tolylsulfide by *tert*-butylhydroperoxide using complexes **1**–**3** as catalysts was investigated (Scheme 3). The reactions were run in CD_3CN solutions at 25 °C at 1 mol% catalysts loadings, and the yields of sulfoxide were monitored via ^{1}H NMR measurements at given intervals with the solvent residual signal as internal standard. Control experiments in the absence of catalyst gave no reaction. The catalytic reactions started immediately without any noticeable induction times. No colour change of the solutions were observed over a period of 24 h, suggesting that the catalysts remained intact. A high selectivity for sulfoxide formation was detected, with the corresponding sulfone being formed as a minor product (*ca.* 2–5%). Although both the catalysts and sulfoxide product are chiral (*vide supra*), the potential enantioselectivites of the reactions were not evaluated as racemates of the molybdenum catalysts were used at all times. The results are summarized in Table 5.

Table 4
Yields (%) of $OPPh_3$ with DMSO to PPh_3 after 20/40 h[a].

DMSO	1	2	3
20 h	65	20	85
40 h	90	40	>99

[a] Conditions: 5 mol % catalyst at 65 °C.

All three complexes were found to catalyse sulfide oxidation with moderate yields. The catalytic efficiencies, as measured in product yields, are in the order **1** > **3**>**2**. Again, we attribute the relatively low reactivity of **2** primarily to steric reasons.

4.3. Catalytic epoxidation

Complexes **1**–**3** were tested as catalysts in the epoxidation of five olefinic substrates, *viz. cis*-cyclooctene, 1-octene, styrene, limonene and α-terpineol (Fig. 5). In the case of the two latter substrates, racemic mixtures of the R- and S-enantiomers were used.

The catalytic epoxidation reactions were conducted with 1 mol% catalyst loading in $CHCl_3$ at 50 °C with 3 equiv. of *tert*-butyl hydroperoxide (TBHP) oxidant with respect to alkene substrate. The progress of the catalytic reactions was monitored by withdrawing aliquots of the reaction mixtures during the reactions and subjecting them to GC-MS analysis. The results are shown in Table 6.

Complex **2** showed the overall poorest catalytic activity, only displaying mediocre activity in the epoxidation of *cis*-cyclooctene. For 1-octene no conversion of substrate could be observed, whereas for the substrates styrene, limonene and α-terpineol no selectivity for the respective epoxides were observed in experiments with complex **2**. Complexes **1** and **3** showed a slightly better catalytic reaction profile for the challenging substrates 1-octene and limonene. Similar to **2**, both complexes **1** and **3** did not show any selectivity in the epoxidation of styrene; only benzaldehyde was observed as the major product, the result of over-oxidation. In the epoxidation of 1-octene, complexes **1** and **3** gave very poor activities and selectivities, with 2-octanone being the major side-product. Interestingly, for limonene rather good activities were observed, with a high selectivity towards the epoxidation of the endocyclic double bond of limonene. For complex **3**, traces of limonene dioxide (∼3%), *i.e.* epoxidation of both the endocyclic and exocyclic double bonds, could be detected. In contrast to limonene, the epoxidation of α-terpineol yields a mix of several oxidation products and only trace quantities of the desired epoxide. It appears that the hydroxy group of α-terpineol interferes with catalytic activity. Attempts to replace TBHP with the more eco-friendly oxidant H_2O_2 did not result in conversion of any substrate when experiments were carried out under the same conditions as with TBHP. This is in contrast to the observations by Peng who found the analogue $[MoO_2(L^2)(MeOH)]$ to be a good epoxidation catalyst for cyclooctene and styrene in an $MeOH/CH_2Cl_2$ mixture when H_2O_2 was used as an oxidant in the presence of base ($NaHCO_3$) [34].

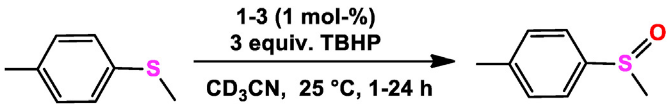

Scheme 3. Dioxidomolybdenum (VI) catalysed oxidation of methyl-*p*-tolylsulfide.

Table 5
Sulfoxidation of methyl-*p*-tolylsulfide using TBHP.

	1	**2**	**3**	T
	Yield [%]	Yield [%]	Yield [%]	
TBHP	75	55	67	24 h

Reaction conditions: Yield of the product measured by ^{1}H NMR spectroscopy. 1 mol % of catalyst (**1**–**3**), 3.0 equivalents of *tert*-BuOOH at 25 °C.

5. Summary and conclusions

In summary, two new *cis*-Mo(VI)O_2 complexes, *viz.* [$MoO_2(L^2)(H_2O)$] (**2**) and [$MoO_2(L^3)(H_2O)$] (**3**), where L^2 and L^3 are tridentate hydrazone-based O,N,O′-donors, have been synthesized and characterized. These two complexes, and the known complex [$MoO_2(L^1)(H_2O)$] (**1**) have been investigated as catalysts for oxygen atom transfer and oxidation reactions. Complexes **1**–**3** are active catalysts for oxygen atom transfer from DMSO to triphenylphosphine and oxidation of methyl-*p*-tolylsulfide using by *tert*-butyl hydroperoxide. Catalytic epoxidation proved to be more difficult, with relative divergent results and poor to non-existent conversions for some of the substrates investigated. Complex **3** proved to be the best overall oxidation catalyst, with complex **2** proving to be consistently the worst catalyst for the reactions that have been studied. The reactivity of **3** may be influenced by the presence of the electron-withdrawing oxime functionality in the hydrazone ligand; this substituent should render the oxido groups of **3** less basic but it should make a presumptive Mo(IV) mono-oxo intermediate formed in the oxo atom transfer reaction more prone to abstract an oxygen atom from the substrate (DMSO). In oxidation reactions employing **3** as a catalyst, the oxime functionality may assist in guiding *tert*-butylhydroperoxide to the complex to form the type of molybdenum peroxido complex that has been proposed to be the active oxidant in epoxidation catalysis [38–40]. We ascribe the low reactivity of **2** to be due primarily to steric hindrance imposed by the ligand. Further reactivity studies and computational modelling will be required to fully assess the catalytic properties of the complexes.

6. Experimental section

6.1. Materials and physical measurements

Commercial grade chemicals were used without further purification in the syntheses and HPLC grade solvents were used as purchased. All syntheses and manipulations were performed under ambient laboratory atmosphere. The ^{1}H and ^{13}C NMR spectra were recorded using a Varian Inova 500 MHz spectrometer or Bruker AC-400 400 Mhz spectrometer in deuterated chloroform or dimethylsulfoxide ($CDCl_3$ or DMSO-d_6) solutions at room temperature and referenced to the residual signal of the solvent. Peaks are reported as singlet (s), doublet (d), doublet of doublets (dd), triplet (t) and multiplet (m or unresolved), coupling constants are given in Hz. Samples for infrared spectroscopy were recorded on Bruker Vertex 70 or PerkinElmer Spectrum BX spectrometers with resonances given in wave number (cm^{-1}) and intensities (br = broad, vs = very strong, s = strong, m = medium, w = weak). Mass spectrometry was performed with a Waters ZQ 4000 or Bruker Apex Ultra FT-ICR spectrometer. Results are denoted as cationic mass peaks; unit is the mass/charge ratio.

Table 6
Conversion (selectivity) of epoxide for complexes **1**–**3**.

[%]	**1**	**2**	**3**
cyclooctene, **S1**	83 (77)	33 (94)	>95 (81)[a]
1-octene, **S2**	10 (79)	no conv.	59 (88)
styrene, **S3**	unsel.	unsel.	unsel.
limonene, **S4**	53 (96)	unsel.	58 (96)
α-terpineol, **S5**	unsel.	unsel.	unsel.

General conditions: 1 mol% catalyst, 0.5 ml $CHCl_3$, 50 °C, 3 equiv. TBHP, conversion (selectivity) of epoxide after 24 h; [a] max. conversion of epoxide reached after 4 h.

6.2. Crystallography

The crystals of **2** and **3** were immersed in cryo-oil, mounted in a loop, and measured at a temperature of 123–170 K. The X-ray diffraction data were collected on a Rigaku Oxford Diffraction Supernova diffractometer using Cu Kα (**2**) or Mo Kα (**3**) or radiation. The *CrysAlisPro* [41] software package was used for cell refinements and data reductions. A multi-scan (**2**) or analytical (**3**) absorption correction (*SADABS* [42] (**2**), *CrysAlisPro* [41] (**3**)) was applied to the intensities before structure solution. The structures were solved by charge flipping method using the *SUPERFLIP* [43] software. Structural refinements were carried out using *SHELXL* [44] software with *SHELXLE* [45] graphical user interface. The hydrogen atoms were positioned geometrically and constrained to ride on their parent atoms with C–H = 0.95–0.98, *O*–H = 0.84–0.875 Å and U_{iso} = 1.2–1.5 U_{eq} (parent atom). Crystallographic data for the structures in this paper have been deposited with the Cambridge Crystallographic Data Centre as supplementary publication numbers. The following CCDC deposition numbers were assigned: 2045993 (**2**), 2045994 (**3**). These data can be obtained free of charge from the Cambridge Crystallographic Data Centre via www.ccdc.cam.ac.uk/data_request/cif.

6.3. Catalytic oxygen atom transfer reaction

The oxygen atom transfer reactions to PPh_3 (0.25 mmol) catalysed by complexes **1**–**3** (0.0125 mmol) were run in DMSO-d_6 (0.5 mL) at 65 °C. The reaction progress was monitored by ^{31}P NMR using a 15-min interval. The set of experiments involved PPh_3 reveals that a singlet at −6 ppm was converted to $OPPh_3$ at approx. 27 ppm.

6.4. Epoxidation experiments

Epoxidation experiments were conducted using a Heidolph Parallel Synthesizer. In a typical experiment, 2–3 mg of catalyst (1 mol %) was dissolved in 0.5 mL of $CHCl_3$ and mixed with 1 equiv. of substrate. Then mesitylene was added as internal standard, and the reaction mixtures were heated to 50 °C, whereupon the oxidant (3 equiv.) was added in one

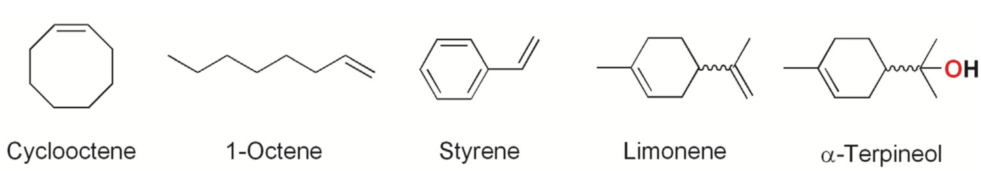

Fig. 5. Alkene substrates used for epoxidation experiments. In the cases of limonene and α-terpineol, racemic mixtures of the R- and S-isomers were used.

portion. Aliquots for GC−MS (20 μL) were withdrawn with a calibrated Socorex Acura 825, 10–100 μL variable volume pipet at given time intervals, quenched with MnO_2, and diluted with HPLC−grade ethyl acetate. The reaction products were analyzed by GC−MS (Agilent Technologies 7890 GC System), and the epoxide produced from each reaction mixture was quantified versus mesitylene as the internal standard.

6.5. Typical procedure for sulfoxidation

Reactions were carried out at room temperature in deuterated acetonitrile solutions using 1:3 molar ratios of substrate/tBuOOH (0.2 M: 0.6 M) and 10 μL of 1,2-dichloroethane added as an internal standard in a 5 mm NMR tube. The reactions were monitored continuously by ^{1}H NMR spectroscopy using a 15-min interval for up to 24 h. The relative intensities of substrate and product resonances were estimated on the basis of the integrated intensities of spectra. Concentrations of the sulfide methyl singlet at 2.45 ppm and the sulfoxide methyl singlet at 2.71 ppm were measured with respect to the internal standard, 1,2-dichloroethane (3.73 ppm).

6.6. Preparation of ligands

Ligands H_2L^1 and H_2L^2 were prepared according to the procedure of Lei and Fu [33].

6.7. Preparation of H_2L^3

N'-(2-hydroxybenzylidene)-2-(hydroxyimino)propanehydrazide (H_2L^3) was synthesized according to a slight modification of a published procedure [46]. A solution of 2-(hydroxyimino)propanehydrazide (1.17 g, 10 mmol), prepared as described elsewhere [47], in methanol (30 mL) was treated with salicylaldehyde (1.22 g, 10 mmol). The resulting mixture was heated under reflux for 1.5 h. On cooling to room temperature, a solid yellowish precipitate was formed. The solid was filtered off, washed with methanol and dried in air. Some additional amount of ligand coud be obtained from the filtrate by partial evaporation of the solvent under vacuum and filtration off the formed precipitate. Yield 2.04 g (92%). Found: C, 54.18; H, 5.10; N, 19.04. Calc. for $C_{10}H_{11}N_3O_3$: C, 54.29; H, 5.01; N, 19.00.^{1}H-NMR (400 MHz, DMSO-d_6) δ 11.74 (1H, s, oxime-OH), 11.62 (1H, s, phenol-OH), 11.39 (1H, s, amide, NH), 8.57 (1H, s, CH), 7.31 (1H, t, $J = 8.0$ Hz), 7.23 (1H, t, $J = 7.4$ Hz), 6.85 (2H, t, $J = 8.8$ Hz), 2.00 (3H, s, CH_3). ^{13}C NMR (126 MHz, DMSO-d_6) δ 160.65 (C═O), 158.04 (C═NOH), 150.20, 149.60, 131.47, 130.34, 119.50, 118.77, 116.79 (Ar–C), 10.03 (CH_3). Selected FT-IR (cm^{-1}) 1659 ($C{=}O_{Amide}$), 1024 ($N\text{-}O_{oxime}$).

6.8. Syntheses of complexes 2 and 3

$[MoO_2(L^2)(H_2O)]$ (**2**): $[MoO_2(acac)_2]$ (0.328 g, 1.0 mmol) was dissolved in methanol and an equimolar quantity (0.367 g, 1.0 mmol) of the ligand H_2L^2 dissolved in the same solvent was added to the solution at room temperature over a period of 2 h to give a deep yellow solution. The resultant solution was kept for two days leading to the formation of well-shaped red single crystals by slow evaporation process at room temperature. Transparent, needle-shaped orange crystals suitable for X-ray analysis were filtered off, washed three times with cold hexane and dried in air. Yield 85% (0.436 g). ^{1}H NMR (500 MHz, DMSO-d_6) δ 8.90 (s, 1H), 7.89 (d, $J = 8.2$ Hz, 2H), 7.63 (d, $J = 2.5$ Hz, 1H), 7.50 (d, $J = 2.5$ Hz, 1H), 7.34–7.30 (m, 2H), 2.38 (s, 3H), 1.36 (s, 9H), 1.30 (s, 9H). ^{13}C NMR (126 MHz, DMSO-d_6) δ 176.24, 164.13, 164.00, 150.70, 149.55, 145.06, 136.94, 136.59, 135.53, 134.84, 127.80 (Ar–C), 42.50, 41.69 [$C(CH_3)_3$], 38.71, 37.06, 28.74 (CH_3). Selected FT-IR (cm^{-1}) 944s (Mo═O), 916s (Mo═O), 1613 ($C{=}O_{Amide}$), 1056 ($N\text{-}O_{oxime}$). ESI-MS: $m/z = 551$ $[MoO_2(L^2)(H_2O)+MeCN]^+$, 511 $[MoO_2(L^2)(H_2O)+H]^+$, 495 $[MoO_2(L^2)+H]^+$, 389 $[H_2L^2+Na]^+$, 369 $[H_2L^2+Na]^+$.

$[MoO_2(L^3)(H_2O)]\cdot 2H_2O$ (**3**): A mixture of H_2L^3 (0.221 g, 1.0 mmol) and $[MoO_2(acac)_2]$ (0.328 g, 1.0 mmol) in 5 mL of methanol was heated to 60 °C for 15 min. After cooling to room temperature, a portion of 10 mL of water was added and the resultant solution was stirred for 1 min. A yellow crystalline precipitate of compound **3** formed during 10–15 min. The resultant product was filtered off, washed with acetone and dried in air. Yield 0.28 g (69%). Yellow single crystals suitable for X-ray analysis were grown by slow evaporation of a methanol-water (1/1, w/w) solution. ^{1}H-NMR (400 MHz, DMSO-d_6, 25 °C): 2.10 (3H, s, CH_3), 6.89 (1H, d, $J = 8.4$ Hz), 7.02 (1H, t, $J = 7.2$ Hz), 7.48 (1H, t, $J = 7.2$ Hz), 7.64 (1H, d, $J = 7.2$ Hz), 8.78 (1H, s, CH), 12.00 (1H, s, oxime-OH). ^{13}C NMR (126 MHz, DMSO-d_6) δ 167.03 (C═O, enolate), 159.52 (C═NOH), 157.05, 147.75, 135.23, 134.47, 121.54, 120.01, 118.61 (Ar–C), 11.29 (CH_3). Selected FT-IR (cm^{-1}) 936s (Mo═O), 912s (Mo═O), 1604 ($C{=}O_{Amide}$), 1020 ($N\text{-}O_{oxime}$). ESI-MS: $m/z = 349.97$ $(\{[MoO_2(L^3)]+H^+\}^+)$, 371.95 $(\{[MoO_2(L^3)]+Na^+\}^+)$, 387.93 $(\{[MoO_2(L^3)]+K^+\}^+)$, 716.92 $(\{2\,[MoO_2(L^3)]+Na^+\}^+)$, 1063.88 $(\{3\,[MoO_2(L^3)]+Na^+\}^+)$.

Notes

The authors declare no competing financial interest.

Declaration of competing interest

The authors declare that they have no known competing financial interests or personal relationships that could have appeared to influence the work reported in this paper.

Acknowledgements

This research has been carried out within the framework of COST Action CM1003 *Biological oxidation reactions - mechanisms and design of new catalysts*. M.K.H. thanks the European Commission for an Erasmus Mundus predoctoral fellowship. E.N and I.F. thank the Swedish Institute for a joint collaborative grant from the Visby program.

Appendix A. Supplementary data

Supplementary data to this article can be found online at https://doi.org/10.1016/j.jics.2021.100006.

References

[1] Arzoumanian H. Molybdenum-oxo chemistry in various aspects of oxygen atom transfer processes. Coord. Chem. Rev. 1998;178–180:191–202.
[2] Brégeault J-M. Transition-metal complexes for liquid-phase catalytic oxidation: some aspects of industrial reactions and of emerging technologies. Dalton Trans. 2003:3289–302.
[3] (a) Kühn FE, Xue W-M, Al-Ajlouni A, Santos AM, Zang S, Romão CC, Eickerling G, Herdtweck E. Synthesis and catalytic application of octahedral lewis base adducts of dichloro and dialkyl dioxotungsten(VI). Inorg. Chem. 2002;41:4468–77.(b) Kühn FE, Groarke M, Bencze É, Herdtweck E, Prazeres A, Santos AM, Calhorda MJ, Romão CC, Gonçalves IS, Lopes AD, Pillinger M. Octahedral bipyridine and bipyrimidine dioxomolybdenum(VI) complexes: characterization, application in catalytic epoxidation, and density functional mechanistic study. Chem. Eur J. 2002; 8:2370–83.(c) Herrmann WA, Fridgen J, Lobmaier GM, Spiegler M. First tungsten complexes with 2′-pyridyl alcoholate ligands: synthesis, structure, and application as novel epoxidation catalysts. New J. Chem. 1999;23:5–7.(d) Wong Y-L, Cowley AR, Dilworth JR. Synthesis, structures, electrochemistry and properties of dioxo-molybdenum(VI) and -tungsten(VI) complexes with novel asymmetric N_2OS, and partially symmetric N_2S_2, NOS_2 N-capped tripodal ligands. Inorg. Chim. Acta. 2004;357:4358–72.
[4] Hille R. The mononuclear molybdenum enzymes. Chem. Rev. 1996;96:2757–816.
[5] Romão MJ. Molybdenum and tungsten enzymes: a crystallographic and mechanistic overview. Dalton Trans. 2009:4053–68.
[6] Schulzke C. Molybdenum and tungsten oxidoreductase models. Eur. J. Inorg. Chem. 2011:1189–99.
[7] Most K, Hoßbach J, Vidović D, Magull J, Mösch-Zanetti NC. Oxygen-transfer reactions of molybdenum- and tungstendioxo complexes containing η2-pyrazolate ligands. Adv. Synth. Catal. 2005;347:463–72.
[8] (a) Hille R. The molybdenum oxotransferases and related enzymes. Dalton Trans. 2013;42:3029–42.(b) Hille R, Hall J, Basu P. Chem. Rev. The mononuclear molybdenum enzymes 2014;114:3963–4038.

[9] Hille R, Nishino T, Bittner F. Molybdenum enzymes in higher organisms. Coord. Chem. Rev. 2011;255:1179–205.
[10] (a) Enemark JH, Cooney JJA, Wang J-J, Holm RH. Synthetic analogues and reaction systems relevant to the molybdenum and tungsten oxotransferases. Chem. Rev. 2004;104:1175–200.(b) Holm RH, Solomon EI, Majumdar A, Tenderholt A. Comparative molecular chemistry of molybdenum and tungsten and its relation to hydroxylase and oxotransferase enzymes. Coord. Chem. Rev. 2011;255:993–1015.
[11] Enemark JH, Garner CD. The coordination chemistry and function of the molybdenum centers of the oxomolybdoenzymes. J. Biol. Inorg. Chem. 1997;2:817–22.
[12] Schrapers P, Hartmann T, Kositzki R, Dau H, Reschke S, Schulzke C, Leimkühler S, Haumann M. Sulfido and cysteine ligation changes at the molybdenum cofactor during substrate conversion by formate dehydrogenase (FDH) from *Rhodobacter capsulatus*. Inorg. Chem. 2015;54:3260–71.
[13] Mitra J, Sarkar S. Oxo-Mo(IV)(dithiolene)thiolato complexes: analogue of reduced sulfite oxidase. Inorg. Chem. 2013;52:3032–42.
[14] Eierhoff D, Tung WC, Hammerschmidt A, Krebs B. Molybdenum complexes with O,N,S donor ligands as models for active sites in oxotransferases and hydroxylases. Inorg. Chim. Acta. 2009;362:915–28.
[15] McNaughton RL, Helton ME, Cosper MM, Enemark JH, Kirk ML. Nature of the oxomolybdenum-thiolate π-bond: implications for Mo-S bonding in sulfite oxidase and xanthine oxidase. Inorg. Chem. 2004;43:1625–37.
[16] Xiao Z, Bruck MA, Enemark JH, Young CG, Wedd AG. A catalytic cycle related to molybdenum enzymes containing $[MoVIO_2]^{2+}$ oxidized active sites. Inorg. Chem. 1996;35:7508–15.
[17] Nemykin VN, Basu P. Oxygen atom transfer reactivity from a dioxo-Mo(VI) complex to tertiary phosphines: synthesis, characterization, and structure of phosphoryl intermediate complexes. Inorg. Chem. 2005;44:7494–502.
[18] Lyashenko G, Saischek G, Pal A, Herbst-Irmer R, Mösch-Zanetti NC. Molecular oxygen activation by a molybdenum(IV) monooxo bis(β-ketiminato) complex. Chem. Commun. 2007:701–3.
[19] Volpe M, Mösch-Zanetti NC. Molybdenum(VI) dioxo and oxo-imido complexes of fluorinated β-Ketiminato ligands and their use in OAT reactions. Inorg. Chem. 2012;51:1440–9.
[20] Whiteoak CJ, Britovsek GJP, Gibson VC, White AJP. Electronic effects in oxo transfer reactions catalysed by salan molybdenum(VI) *cis*-dioxo complexes. Dalton Trans. 2009 2337-234, https://pubs.rsc.org/en/content/articlelanding/2009/dt/b820754b#!divAbstract.
[21] Lehtonen A, Sillanpää R. Dioxomolybdenum(VI) complexes with tri- and tetradentate aminobis(phenolate)s. Polyhedron 2005;24:257–65.
[22] Lehtonen A, Wasberg M, Sillanpää R. Dioxomolybdenum(VI) and -tungsten(VI) complexes with tetradentate aminobis(phenol) ligands. Polyhedron 2006;25:767–75.
[23] Pramanik NR, Ghosh S, Raychaudhuri TK, Ray S, Butcher RJ, Mandal SS. Synthesis, characterization and crystal structure of oxomolybdenum(VI) and (IV) complexes of some tridentate ONS donor ligands. Polyhedron 2004;23:1595–603.
[24] Dinda R, Sengupta P, Ghosh S, Sheldrick WS. Synthesis, structure, and reactivity of a new mononuclear molybdenum(VI) complex resembling the active center of molybdenum oxotransferases. Eur. J. Inorg. Chem. 2003:363–9.
[25] Moroz YS, Kulon K, Haukka M, Gumienna-Kontecka E, Kozłowski H, Meyer F, Fritsky IO. Synthesis and structure of [2 × 2] molecular grid copper(II) and nickel(II) complexes with a new polydentate oxime-containing Schiff base ligand. Inorg. Chem. 2008;47:5656–65.
[26] Kasuga NC, Sekino K, Koumo C, Shimada N, Ishikawa M, Nomiya K. Synthesis, structural characterization and antimicrobial activities of 4- and 6-coordinate nickel(II) complexes with three thiosemicarbazones and semicarbazone ligands. J. Inorg. Biochem. 2001;84:55–65.
[27] Leigh M, Castillo CE, Raines DJ, Duhme-Klair AK. Synthesis, activity testing and molybdenum(VI) complexation of Schiff bases derived from 2,4,6-trihydroxybenzaldehyde investigated as xanthine oxidase inhibitors. ChemMedChem 2011;6:612–6.
[28] Leigh M, Raines DJ, Castillo CE, Duhme-Klair AK. Inhibition of xanthine oxidase by thiosemicarbazones, hydrazones and dithiocarbazates derived from hydroxy-substituted benzaldehydes. ChemMedChem 2011;6:1107–18.
[29] Pisk J, Prugovečki B, Matcović-Čalogović D, Poli R, Agustin D, Vrdoljak V. Charged dioxomolybdenum(VI) complexes with pyridoxal thiosemicarbazone ligands as molybdenum(V) precursors in oxygen atom transfer process and epoxidation (pre) catalysts. Polyhedron 2012;33:441–9.
[30] Jin N-Y. Syntheses, crystal structures, and catalytic properties of dioxomolybdenum(VI) complexes with hydrazone ligands. J. Coord. Chem. 2012;65:4013–22.
[31] He X-Q. Syntheses, X-ray structures, and catalytic oxidations of dioxomolybdenum(VI) complexes with tridentate benzohydrazones. J. Coord. Chem. 2013;66:966–76.
[32] Lei Y, Yang Q, Chen G, Yang Q. Synthesis, X-ray structural characterization, and catalytic property of dioxomolybdenum(vi) complexes with N'-(3-bromo-2-hydroxybenzylidene)-2-hydroxybenzohydrazide and N'-(5-chloro-2-hydroxybenzylidene)-4- nitrobenzohydrazide. Synth. React. Inorg. Metal-Org. Nano-Metal Chem. 2014;44:590–7.
[33] Lei Y, Fu C. Synthesis and X-ray structural characterization of dioxomolybdenum(VI) complexes with N'-(5-chloro-2-hydroxybenzylidene)-4-methylbenzohydrazide and N'-(2-hydroxybenzylidene)-4-methylbenzohydrazide. Russ. J. Coord. Chem. 2012;38:65–70.
[34] Peng D-L. Crystal structure and catalytic property of an oxidomolybdenum(vi) complex derived from N'-(2-hydroxy-3,5-di-tert-butylbenzylidene)-4-methylbenzohydrazide. J. Struct. Chem. 2018;59:589–94.
[35] Ghorbanloo M, Bikas R, Małecki G. New molybdenum(VI) complexes with thiazole-hydrazone ligand: preparation, structural characterization, and catalytic applications in olefin epoxidation. Inorg. Chim. Acta. 2016;445:8–16.
[36] Pisk J, Prugovečki B, Matcović-Čalogović D, Jednačak T, Novak P, Agustin D, Vrdoljak V. Pyridoxal hydrazonato molybdenum(VI) complexes: assembly, structure and epoxidation (pre)catalyst testing under solvent-free conditions. RSC Adv. 2014;4:39000–10.
[37] Alghool S, Slebodnick C. Supramolecular structures of mononuclear and dinuclear dioxomolybdenum(VI) complexes via hydrogen bonds and π-π stacking, thermal studies and electrochemical measurements. Polyhedron 2014;67:11–8.
[38] (a) Mimoun H, de Roch IS, Sajus L. Epoxidation of olefins with covalent peroxomolybdenum(VI) complexes. Tetrahedron 1970;26:37–50.(b) Deubel DV, Sundermeyer J, Frenking G. Mechanism of the olefin epoxidation catalyzed by molybdenum diperoxo complexes: quantum-chemical calculations give an answer to a long-standing question. J. Am. Chem. Soc. 2000;122:10101–8.(c) Deubel DV, Frenking G, Gisdakis P, Herrmann WA, Rösch N, Sundermeyer J. Olefin epoxidation with inorganic peroxides. solutions to four long-standing controversies on the mechanism of oxygen transfer. Acc. Chem. Res. 2004;37:645–52.
[39] (a) Kagan HB, Mimoun H, Marc C, Schurig V. Asymmetric epoxidation of simple olefins with an optically active molybdenum(VIi) peroxo complex. Angew. Chem., Int. Ed. Engl. 1979;18:485–6.(b) Deubel DV, Sundermeyer J, Frenking G. In search of catalytically active species in the surfactant-mediated biphasic alkene epoxidation with Mimoun-type complexes. Org. Lett. 2001;3:329–32.
[40] Sharpless KB, Townsend JM, Williams DR. Mechanism of epoxidation of olefins by covalent peroxides of molybdenum(VI). J. Am. Chem. Soc. 1972;94:295–6.(b) Chong AO, Sharpless KB. Mechanism of the molybdenum and vanadium catalyzed epoxidation of olefins by alkyl hydroperoxides. J. Org. Chem. 1977;42:1587–90.
[41] Rigaku Oxford Diffraction. CrysAlisPro. Oxfordshire, England: Yarnton; 2019. Agilent Technologies inc.
[42] Sheldrick GM. SADABS - Bruker Nonius Scaling and Absorption Correction -. Madison, Wisconsin, USA: Bruker AXS, Inc.; 2008.
[43] Palatinus L, Chapuis G. SUPERFLIP. A computer program for the solution of crystal structures by charge flipping in arbitrary dimensions. J. Appl. Crystallogr. 2007;40:786–90.
[44] Sheldrick GM. Acta Crystallogr. 2015;C71:3–8.
[45] Hübschle CB, Sheldrick GM, Dittrich B. ShelXle: a Qt graphical user interface for SHELXL. J. Appl. Crystallogr. 2011;44:1281–4.
[46] Plutenko MO, Lampeka RD, Moroz YS, Haukka M, Pavlova SV. N'-(2-Hydroxybenzylidene)-2-(hydroxyimino)propanohydrazide. Acta Crystallogr. 2011;E67:o3282–3.
[47] Fritsky IO, Kozłowski H, Sadler PJ, Yefetova OP, Świątek-Kozłowska J, Kalibabchuk VA, Głowiak T. Template synthesis of square-planar nickel(II) and copper(III) complexes based on hydrazide ligands. J. Chem. Soc., Dalton Trans. 1998:3269–74.